Preprint

Brain signal complexity and aperiodicity predict human corticospinal excitability

Joel Frohlich[1,2,+], Simon Ruch[1,3,+], Bettina H. Trunk[1], Marius Keute[1], Pedro A.M. Mediano[4], and Alireza Gharabaghi[1,5,6]

[1]Institute for Neuromodulation and Neurotechnology, University Hospital and University of Tübingen, Germany; [2]Institute for Advanced Consciousness Studies, Santa Monica, California, USA; [3]Faculty of Psychology, UniDistance Suisse, Brig, Switzerland; [4]Department of Computing, Imperial College London, London, UK; [5]Center for Bionic Intelligence Tübingen Stuttgart (BITS), Germany; [6]German Center for Mental Health (DZPG), 72076 Tübingen, Germany ; [+]These authors contributed equally to this work

This manuscript was written in LaTeX and compiled on February 9, 2024

Abstract

Transcranial magnetic stimulation (TMS) is a frequently used intervention for brain modulation with highly promising scientific and therapeutic applications. Two shortcomings of TMS applications, however, are the high within-subject and between-subjects variability in response to stimulation, which undermine the robustness and reproducibility of results. A possible solution is to optimize individual responses to TMS by exploiting rapidly fluctuating state variables such as the phase and power of neural oscillations. However, there is widespread uncertainty concerning the appropriate frequency and/or phase to target. Here, we evaluate two different approaches which do not require a choice of frequency or phase but instead utilize properties of the broadband EEG signal to predict corticospinal excitability (CSE). Our results suggest that both the spectral exponent (i.e., the steepness of the EEG 1/f background or aperiodic component) and the entropy or "complexity" of the EEG signal are both useful predictors of CSE above and beyond band-limited features, and may be deployed in brain state-dependent TMS applications.

TMS | EEG | Entropy | Spectral exponent | Aperiodic activity | Corticospinal excitability |Motor cortex

Please address correspondence to: Alireza Gharabaghi (alireza.gharabaghi@uni-tuebingen.de) or Joel Frohlich (jfneuro@pm.me).

Introduction

The refinement of scientific and therapeutic applications of transcranial magnetic stimulation (TMS) hinges on the temporal alignment of stimuli with heightened periods of brain responsiveness. To achieve this, TMS pulses may be guided by concurrently recorded cortical oscillations using electroencephalography (EEG). However, a substantial challenge lies in the uncertainty surrounding the optimal frequency and phase for triggering stimulation. Existing literature often presents inconclusive or conflicting findings.

Exploration into the state-dependency of corticospinal excitability (CSE) has manifested in three investigative approaches. First, studies have employed post-hoc analyses of randomly administered TMS pulses. Second, frequency-specific transcranial alternating current stimulation (tACS)

has been combined with phase-specific TMS. Finally, EEG-triggered TMS has been applied to selectively target specific frequencies and phases.

Post-hoc analyses allow one to investigate a broad range of frequencies in an exploratory way, but are often confronted with methodological challenges in data processing (1) and require large sample sizes to identify state-dependency due to the heterogeneity in phase distribution of the randomly applied TMS pulses. These studies have usually found no frequency or phase-dependency of CSE (2) or identify the beta band and the trough/rising flank of the oscillatory cycle as optimal for CSE (3, 4). In the alpha band, usually no phase-dependency is detected (3, 4), or the rising flank is identified as the optimal phase, when a pre-selected subsample (i.e., the top tertile of subjects ranked by alpha power) is analyzed (5). In these cases, CSE may not depend on phase or power per se, but rather on a significant phase/power interaction, with optimal CSE corresponding to high power and the trough phase of the alpha (mu) rhythm (6, 7) and a reversed direction of phase-dependency with changing alpha power levels (6).

The tACS-TMS approach has also identified phase-dependency of CSE in the beta band, often in the trough/rising flank (8–10), but see also results from Nakazone et al. (11) and Wischnewski et al. (12). In the alpha band, either no phase-dependency is detected (10) or a similar phase-dependency is detected as for the beta band (12).

For EEG-triggered TMS investigations, most methodologies have employed prediction algorithms to address the inherent latency between brain state measurement and stimulation delivery. Consequently, these approaches have been imprecise, i.e., phases in the alpha band are targeted with a standard deviation (SD) of approximately 50° (13, 14). Given this imprecision, many studies have tended to focus on exploring only two opposing phases, such as peak versus trough, within lower frequency oscillations like the alpha (mu) band. This strategic limitation arises from inherently less temporal precision demands associated with lower frequency oscillations compared to their higher frequency counterparts like the beta band. However, this methodological constraint poses a notable challenge when heightened precision (e.g., targeting 45° phase bins(15)) is imperative for achieving specific stimulation effects.

When the trough or peak of the oscillatory alpha cycle is targeted in participants selected on the basis of their elevated sensorimotor alpha power, higher CSE was observed for the trough condition (13). However, this finding was not replicated, when employing the same approach without prescreening individuals according to alpha power (14, 16). Furthermore, recent work suggests significant phase/power interaction in the alpha band (17), while other studies do not observe this relationship (18, 19). Addressing these discrepancies, emerging evidence suggests that pericentral alpha (mu) activity is predominantly localized in the postcentral somatosensory cortex and may therefore influence CSE only indirectly (16, 20). Accordingly, TMS triggered by alpha (mu) activity from the primary motor cortex (M1) has resulted in no phase-dependency (20) or opposite phase effects for the alpha and beta band on CSE (19). Furthermore, nuanced differences in the methodological choices may crucially influence one's sensitivity to detect the relationship between power, phase and CSE (16) and even lead to erroneous phase estimations (1).

A recent advancement in EEG-triggered TMS (21) leverages a non-predictive, real-time integrated measurement and stimulation approach to achieve precise, phase-specific targeting with minimal standard deviations (0.4° at 4 Hz to 4.3° at 40 Hz). Utilizing this technique to target eight phases across ten frequencies (4-40 Hz) revealed consistent, phase-dependent effects, particularly a sinusoidal CSE modulation at 24 Hz, with optimal CSE at the transition from the trough to the rising flank, observed both within and across sessions and individuals (22). Notably, a post-hoc analysis in another study confirmed this sinusoidal modulation exclusively between 23 and 25 Hz (23). However, the technology enabling such temporally precise real-time stimulation is not widely available at present, thus motivating non-phase dependent approaches.

Taken together, the foregoing studies suggest the need for less heavily parameterized EEG features that determine CSE to guide state-dependent TMS and bring it into broad application. With this motivation, we explore two new approaches, one based on EEG signal entropy or "complexity", and another based on the spectral exponent or "steepness" of the EEG 1/f background. Both measures are computed from the broadband EEG signal and thus avoid the pitfalls of approaches which require the selection of a particular frequency band such as alpha or beta. Notably, these broadband EEG measures are also derived from longer EEG windows (nearly a full second) than those used to estimate oscillatory phase or power, a fact which may reduce artifact susceptibility but also sensitivity to short fluctuations in CSE. In this sense, broadband EEG measures may be complimentary, rather than alternative, to conventional band-limited EEG measures, and for this reason,

we investigated the value of both types of EEG features for identifying states of high/low excitability using offline analyses of TMS-EEG data recorded without state targeting.

Our first broadband EEG approach, entropy, can be conceptualized as the number of possible states of the signal, or its "diversity". We computed entropy using both the Lempel-Ziv (LZ) compression algorithm (24) and the context tree weighting (CTW) algorithm (25) to obtain two distinct estimates of signal complexity. More complex or diverse signals are harder to compress, as they contain more information. A broad literature of both theoretical (26–29) and empirical studies (30–34) suggest that high cortical entropy, as measured using EEG or magnetoencephalography (MEG), relates to high capacity for information processing or motor responsiveness. We therefore hypothesized that high motor cortical entropy should predict high CSE.

Our second broadband EEG approach is the spectral exponent (SE) (35), sometimes referred to as the power law exponent, spectral slope, or aperiodic component (36). Evidence from a variety of experiments (37–39) demonstrates that SE increases with greater neural inhibition and decreases with greater neural excitation. As such, we hypothesized that low SE measured from motor cortical EEG signals should predict high CSE.

Materials and Methods

Data collection . We utilized available data from 36 healthy right-handed subjects (M = 24.5, SD = 3.25 years, 11 male) that were acquired after approval by the local ethics committee. Subjects gave written informed consent prior to participation according to the Declaration of Helsinki and had no contraindications to TMS (40).

TMS was applied using a MagPro-R30 stimulator with a MCF-B70 Butterfly Coil (MagVenture GmbH, Denmark) in combination with a neuronavigation system (Localite GmbH, Germany). Participants were seated in an armchair with their forearms pronated and fully relaxed. 64-channel EEG was recorded at 5000 Hz during stimulation (Braincap for TMS, Easycap GmbH, Germany; Brain Products DC amplifiers, BrainProducts GmbH, Germany). EMG of the right EDC was recorded at 5000 Hz with a BrainProducts ExG amplifier (BrainProducts GmbH, Germany) and Ag/AgCI AmbuNeuroline 720 wet gel surface electrodes (Ambu GmbH, Germany). Impedances were kept below 10 $k\Omega$. After recording EEG and EMG, the signals were downsampled and saved at 2000 Hz.

The stimulation site targeting the right EDC was determined prior to each experimental session. For this, 40 stimuli were applied to the left motor cortex with an initial intensity of 40% maximum stimulator output (MSO). In case this intensity was insufficient to elicit MEPs, it was increased in steps of 5% MSO. At the three stimulation sites that resulted in the highest peak-to-peak amplitudes, three additional stimuli were applied. Of these, the stimulation site resulting in the most consistent and highest amplitude MEP was then considered as the motor hotspot. Next, the resting motor threshold (RMT) was determined, which was defined as the lowest intensity that resulted in at least 5 MEP out of 10 stimuli (41). Finally, we stimulated at seven different intensities (i.e., 90 – 150% RMT, in steps of 10% RMT) with 10 trials at each intensity. Blocks of the same intensity were applied in random order.

Data cleaning and preprocessing. Data were imported into MATLAB R2022a (MathWorks, Natick, MA, USA) for preprocessing and analysis. Recordings from separate sessions were combined into single datasets for each participant. For one participant, we were unable to include a subset of sessions due to data corruption issues. Stimulation trigger annotations were corrected to adjust for a 6 ms delay. Stimulation artifacts in EEG and EMG recordings were then interpolated prior to filtering. This was accomplished by 1) replacing the stimulation artifact (50.5 ms duration) with Not-a-Number (NaN) elements, 2) applying a 75 ms moving average filter to smooth a copy of the signal (MATLAB: movmean with 'omitnan' option), and 3) replacing NaN elements of the original, unsmoothed signal with the corresponding section from the smoothed signal. Next, filters were implemented using finite-impulse response (FIR) filtering (filter order = 8000, i.e., 4 x sampling rate). EEG recordings were then bandpass filtered 1 - 40 Hz (EEG), and EMG recordings were first notch filtered at 50 Hz (to attenuate linenoise) and then bandpass filtered 4 - 100 Hz.

Following filtering, EEG data were cleaned using ASR with the following parameters: ChannelCriterion = 0.7, LineNoiseCriterion = 4, BurstCriterion = 3, WindowCriterion = 0.3, ChannelCriterionMaxBadTime = 0.5, BurstRejection = 'off', Highpass = 'off'. ASR was chosen for this cleaning step because it can be used in real-time situations (42), giving findings from this experiment greater translatability to state-dependent TMS applications. Channels marked bad by ASR were spherically interpolated. Next, data were epoched 1000 ms pre-pulse to 200 ms post-pulse and baseline corrected. Finally, to further

clean data, a group-level ICA decomposition was performed using the fastica algorithm on all concatenated EEG data downsampled to 125 Hz. Following the group-level ICA decomposition, we removed one component corresponding to a blink artifact, one component corresponding to a saccade artifact, four components corresponding to muscle artifacts, and eight components possibly corresponding to mechanical artifacts resulting from contact between the TMS coil and electrodes (see Fig. S1). Finally, clean recordings were current source density transformed using the spherical spline method implemented with the publicly available SCD plugin for EEGLAB (43).

EMG measures. Using EMG recorded from the right EDC, we computed MEP amplitudes as maximum peak-to-peak amplitudes within 15-50 ms after TMS stimulation. Trials were rejected in case of muscle pre-activation > 20 µV within 100 ms before the pulse. Additionally, MEPs with amplitudes of less than 20 µV were discarded and MEPs between 20-50 µV were visually inspected. We then log_{10} transformed MEP amplitudes prior to entering them into models. Additionally, we computed the standard deviation of the EMG signal from the right EDC for each trial and entered the log_{10} transformed standard deviation as a covariate into models accounting for muscle activation (see "Statistical analysis" below).

Spectral EEG measures. All spectral measures were computed using the FOOOF algorithm by (36) . For each EEG channel and trial computed the power spectral density (PSD) using the EEG signal from 1000 to 50 ms prior to stimulus onset with the pwelch() function in MATLAB [input parameters: WINDOW = 512, NOVERLAP = 256, F = linspace(1,40,100)]. We then modeled the PSD between 1 and 40 Hz using FOOOF with the 'fixed' approach to parameterizing the aperiodic component (i.e., the 1/f background) and 0.6 and 1.0 Hz as the lower and upper bounds, respectively, for fitted peak widths.

Having modeled the EEG PSD using FOOOF, SE was returned in the aperiodic model parameters. SE is the slope of the aperiodic component modeled by FOOOF, which is the EEG 1/f background, so named because its power is inversely related to frequency (44). When frequency and power are plotted in logarithmic coordinates and spectral peaks are subtracted, the 1/f background shows a linear relationship with frequency (45). It is then straightforward to compute SE as the slope of the 1/f background. Because this slope is nearly always negative, SE is reported as an absolute value.

To identify the alpha peak frequency in a given trial and channel, we then looked for oscillatory components returned by FOOOF with peak frequencies between 8 and 13 Hz. If more than one oscillatory component with a peak frequency in this range was returned, we used the component with the peak frequency closest to 10 Hz. The alpha band was then defined for that trial and channel as f +/- 2 Hz, where f is the peak frequency. In the case that no oscillatory component was returned in the alpha range, we defined the alpha band as 8 - 12 Hz.

Similarly, to identify the beta peak frequency in a given trial and channel, we looked for oscillatory components returned by FOOOF with peak frequencies between 14 and 30 Hz. If more than one oscillatory component was returned in this range, we used the component with the peak frequency closest to 20 Hz. The beta band was then defined for that trial and channel as f +/- 4 Hz, where f is the peak frequency. If no oscillatory component was returned in the beta range, we defined the beta band as 16 - 24 Hz.

Having defined the alpha and beta band for the trial and channel under consideration, to extract alpha and beta power, we then computed the PSD of each filtered signal using the pwelch() function [input parameteres: F = linspace(0,30,128) and default values for WINDOW and NOVERLAP]. Alpha and beta power were computed using trapezoidal integration of the PSD between the appropriate limits of integration for each band, and this power estimate was then log-scaled. Finally, to extract the alpha and beta phase of each EEG signal, we applied the fast Fourier transform to a Hanning windowed segment of signal corresponding to twice the period of the trial-specific alpha or beta center frequency (2) taken from the end of the signal, stopping 50 ms before the TMS pulse. For example, if the EEG alpha band was determined by FOOOF as 9 - 13 Hz, we applied FFT to the signal from -232 to -50 ms relative to the TMS pulse, based on a center alpha frequency of 11 Hz and period of 90.9 ms. We then extracted the phase of the Fourier spectrum corresponding to the alpha or beta center frequency (e.g., in the example given above, the 11 Hz alpha phase). Next, we adjusted the phase estimate to correct for the fact that the FFT window ended 50 ms before the TMS pulse (e.g., if the frequency extracted by FOOOF was 10 Hz, then we added 180° to the phase estimate).

Entropy analysis . Entropy is commonly defined as the number of possible configurations of a system (e.g., thermodynamic entropy). A common approach to estimating signal entropy

is to apply a compression algorithm to the signal following a symbolic transformation (e.g., discretization using quantiles). More complex or diverse signals are harder to compress, as they contain more information. Indeed, entropy and information are intimately related and, in some frameworks (46, 47), identical. We estimated signal entropy for each EEG channel and trial using the EEG signal from 1000 to 50 ms prior to stimulus onset (i.e., 0.95 s of data). To speed up computations, signals were first downsampled to 200 Hz. CTW entropy was computed by transforming each EEG signal into discrete octiles and then applying the CTW compression algorithm (25) to estimate the entropy rate (48). LZ entropy was computed by transforming the signal into two discrete states based on a median split of time series values. We then applied the LZ76 algorithm (i.e., the first in a series of Lempel-Ziv compression algorithm published in 1976) to estimate the signal's entropy (24). Because all trials had the same signal length, we did not normalize the entropy estimate according to signal length.

Statistical analysis. We used linear mixed models (LMMs) to predict log-scaled MEP amplitude with random intercepts for participants and fixed effects for the EEG feature of interest as well as pulse intensity (measured as percent MSO), pulse number, (i.e., the chronological index of the TMS pulse, which controls for habituation and facilitation effects), and the log-scaled standard deviation of the pre-pulse EMG recorded from the right EDC muscle (to control for muscle activation). All LMMs also accounted for interactions between pulse intensity and pulse number, as well as pulse intensity and muscle activation.

To test K predictors of CSE in data containing N trials across n participants, we used separate LMMs at each channel with the formula

$$y = X\beta + Zu + \varepsilon \quad [1]$$

where y is the N x 1 vector of log-scaled MEP amplitudes (i.e., proxies for CSE) for each trial, X is the N x K matrix of fixed effects, including a fixed intercept term (first column), the EEG predictor (second column), the pulse intensity (third column), the pulse number (fourth column), the log-scaled standard deviation of the prepulse EMG signal (fifth column), and interactions of fixed effect terms (subsequent columns); β is the K x 1 vector of fixed effect coefficients, Z is the N x n design matrix of random effects, u is the n x 1 vector of random intercepts, and ε is the N x 1 vector of residuals. Note that in cases where the alpha or beta phase was used to predict CSE, we included two separate columns for the EEG predictor, one corresponding to the sine of the phase and the other corresponding to the cosine of the phase.

To assess the extent to which broadband EEG measures improved the prediction of CSE above and beyond that of conventional band-limited EEG features, we compared the model fit achieved beta features (power and phase) as the EEG terms to a larger model with an additional EEG predictor term corresponding to either signal entropy (LZ or CTW) or SE. We compared the model fit of the larger model to the smaller, nested model using log-likelihood ratio tests.

To correct for multiple testing across 64 EEG channels, we utilized threshold free cluster enhancement (TFCE) (49) using parameters E = 2/3 and H = 2 as recommended by Mensen and Khatami (50). This approach privileges channels surrounded by neighboring channels showing similar effects yet departs from previous cluster statistical approaches (51) by taking many different thresholds into consideration, rather than a single arbitrary threshold which determines clusters. In our case, we sampled 50 evenly spaced thresholds for test statistics starting from 0 and increasing to the largest test statistic present in the data (as judged by absolute value). We then used permutation testing to derive an empirical P-value for each electrode. Data were permuted by randomly shuffling the outcome variable, i.e., MEP amplitudes, for each of 200 permutations. For all thresholds explored, channels were considered neighbors if they fell within 55 mm of one another in the Euclidian space of a 3-dimensional standard template.

To assess the extent to which the predictive power of an EEG feature was driven by within-subject variance (i.e., a state marker) or between-subject variance (i.e., a trait marker), we derived ICCs according to the definition "ICC(l) for Case 1" given in McGraw and Wong (52) with publicly available code (53). We then took the quantity 1 - ICC to be high when a feature was a state marker and low when a feature was a trait marker (see Fig. 5).

Results

Following preprocessing, data from two participants were rejected outright due to an excessive number of noisy channels (exceeding 15% of the total number of channels, i.e., at least 10 noisy channels) identified using ASR. For each remaining participant, TMS trials were rejected based on MEP criteria (see Materials and Methods). A mean of 45 trials were rejected per participant (min = 5, max = 107, median = 42.5). The final

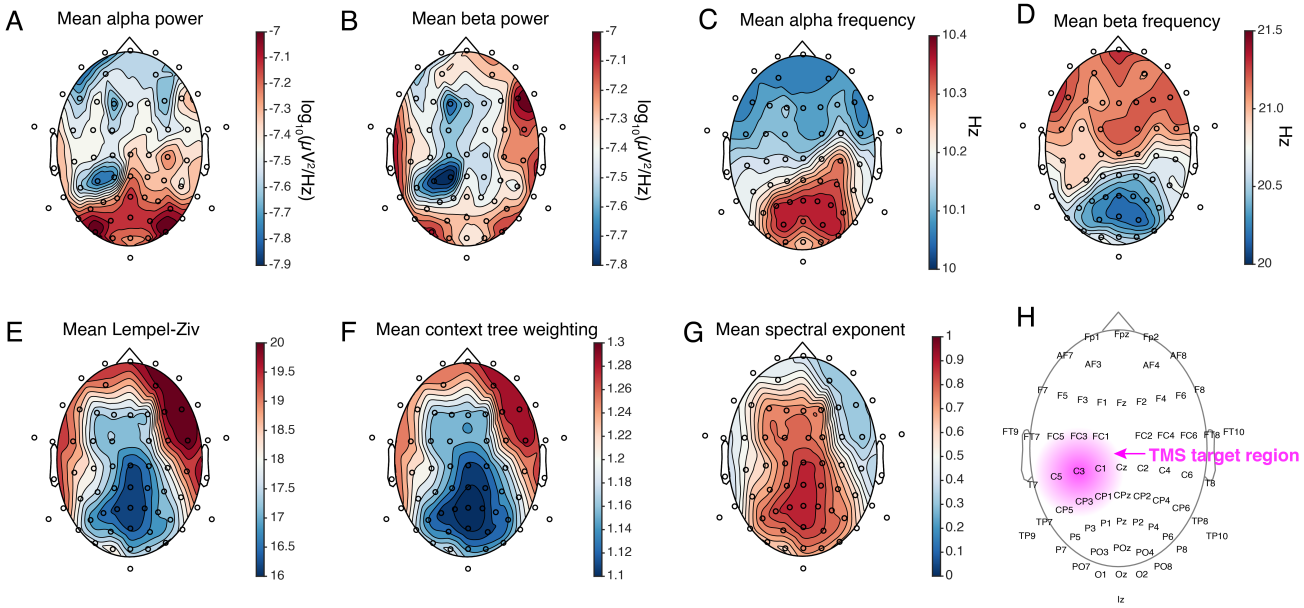

Figure 1. Topographic distributions of EEG features. Alpha power (A) shows a very different distribution than beta power (B). On the other hand, alpha frequency (C) and beta frequency (D) show similar topographies that appear to be mirror images of one another. Broadband EEG measures (E-G) also show remarkably similar scalp topographies with one another; entropy features (E,F) appear as the mirror image of the spectral exponent (G). EEG channel names are indicated in (H), as well as the TMS target region (magenta); note that this is an approximation and not based on real hotspot mapping data.

clean dataset consisted of 8972 TMS trials across 34 participants, with a mean of 264 trials per participant (min = 45, max = 541, median = 237.5).

Having cleaned data, we estimated alpha and beta power, phase, and mean frequency, as well as broadband EEG features CTW, LZ, and SE, for each participant, channel, and trial. We then visualized spatial distributions of relevant EEG features across the scalp (Fig. 1). As expected, EEG alpha power was highest over posterior regions and lowest over anterior regions (Fig. 1A). EEG beta power followed a different spatial distribution, with the highest power over peripheral scalp regions (Fig. 1B). We observed a spatial minimum of beta power at channel CP1, immediately posterior to the stimulation site, which may be related either to cumulative stimulation effects or to artifact removal using ICA.

We also visualized the mean alpha and beta frequency across participants at each channel. By default, we defined the alpha band as 8 - 12 Hz and the beta band as 16 - 24 Hz, but using the fitting oscillations and one-over-f (FOOOF) algorithm (36), we adjusted these frequency ranges in a data-driven manner according to power spectral peaks for each channel of each participant's EEG data (see Materials and Methods). If a spectral peak could not be identified, then the alpha and beta band ranges defaulted to those stated above. However, if a peak was identified near 10 Hz (alpha) or 20 Hz (beta), we took the peak frequency +/- 8 Hz as the frequency range, albeit with a limit imposed such that the range could not exceed 8 - 13 Hz (alpha) or 14 - 30 Hz (beta). This ensured that the frequency bands used in each case stayed within canonical limits.

To visualize the results of this approach, we viewed topographies of the middle most frequency in the alpha (Fig. 1C) and beta (Fig. 1D) band, averaged across participants. The alpha band showed higher frequencies over posterior scalp areas, whereas for the beta band, we observed the opposite sagittal gradient.

Next, we visualized the spatial distribution of the broadband measures LZ, CTW, and SE, which all yielded remarkably similar topographies. LZ and CTW (Fig. 1E,F) were both minimal over parietal regions and maximal over frontotemporal regions, whereas SE (Fig. 1G) exhibited the same topography in reverse, with the steepest 1/f background evident over parietal regions and the least steep 1/f background evident over frontotemporal regions.

To visualize the overall strength of each EEG predictor, we first visualized t-statistcs from LMMs in an exploratory fashion for each channel in the vicinity of the TMS target region with the primary goal of determining whether alpha or beta band-limited measures would serve as a better benchmark which broadband EEG features should improve upon; in the case of phase, we used the square root of the F-statistic as a

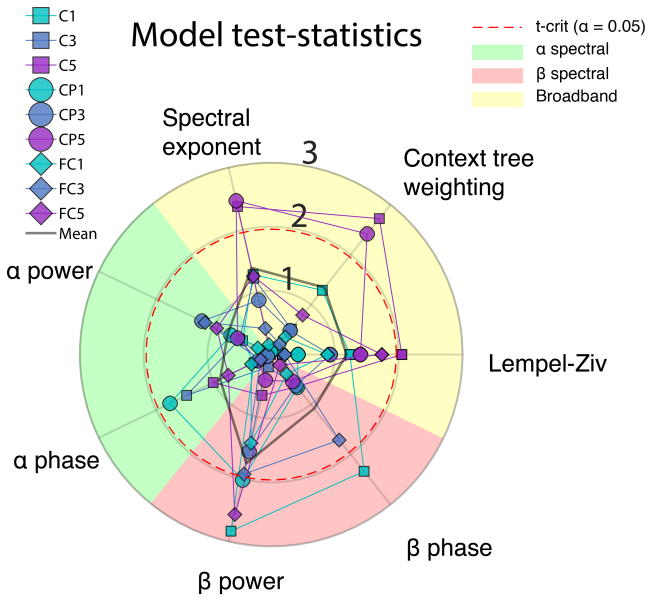

Figure 2.Exploratory visualization of EEG features in the proximity of the TMS target region. In an initial comparison of the predictive ability of different EEG features, we plotted the t-statistic (or$\sqrt{F}$, in the case of phase) from 9 channels in the proximity of the TMS target region (left M1).

proxy for the t-statistic, given that each phase model contained separate t-statistics for the sine and cosine of phase. We plotted these values for channels FC1, FC3, FC5, C1, C3, C5, PC1, PC3, and PC5 (Fig. 2) and divided EEG predictors into three categories: broadband (SE, CTW, LZ), alpha band (power, phase), and beta band (power, phase). Our results demonstrated that beta band features were more predictive than alpha band features (Fig. 2). We thus chose to use beta power and phase as benchmarks against which to test the predictive performance of the broadband EEG measures. For a visualization of test statistics across the entire scalp, see Fig. S2.

We next tested the performance of broadband EEG measures by adding each one to an LMM that already contained beta features and computing a log-likelihood ratio to determine if the additional EEG feature significantly improved model fit. Using TFCE (49), which addresses the multiple comparisons problem while emphasizing channels that show similar effects as neighboring channels, combined with permutation testing to compute empirical P-values for each channel, we identified multiple channels for each broadband measure (SE, CTW, and LZ) that significantly predicted CSE (Fig. 3) and/or significantly improved the fit of models that originally contained only beta power and phase as EEG predictors (Fig. 4).

In what follows, all P-values are reported as corrected using TFCE with permutation testing. First, we examined the predictive power of each broadband EEG measure without adding it to another model. Across a number of electrodes, we found that high SE corresponded to low CSE, whereas high CTW and high LZ corresponded to high CSE (Fig. 3); note one marginally significant peripheral channel (TP9) which showed the opposite effect for CTW and was likely a spurious finding (Fig. 3E). In general, all three measures showed significant effects both in prefrontal and centroparietal scalp regions. However, only SE and CTW showed significant effects in the vicinity of left M1 targeted by TMS, namely, channel C1 (Fig. 3B,D). Given evidence that the postcentral gyrus is the source of the alpha (mu) rhythm believed to modulate sensorimotor excitability (54–57), we next looked immediately posterior to the TMS target region; here, SE and CTW significantly predicted CSE at channels CP1 and CPz (Fig. 3B,D). For exact P-values, see Table S1.

Next, we considered how EEG features could be added to LMMs to improve their prediction of MEP amplitude. An LMM including beta power as the sole fixed effect resulted in strong prediction near the TMS target site, particularly channel C3 (Fig. 4A). Similarly, an LMM with only beta phase fixed effect terms (cos and sin) also showed strong prediction for channel C3 (Fig. 4B); however, when these phase terms were added to a model that already contained beta power, the largest gains were seen at the symmetric scalp site, C4, in the hemisphere contralateral to stimulation, as well as channel FT7 in the ipsilateral hemisphere. We did not consider statistical

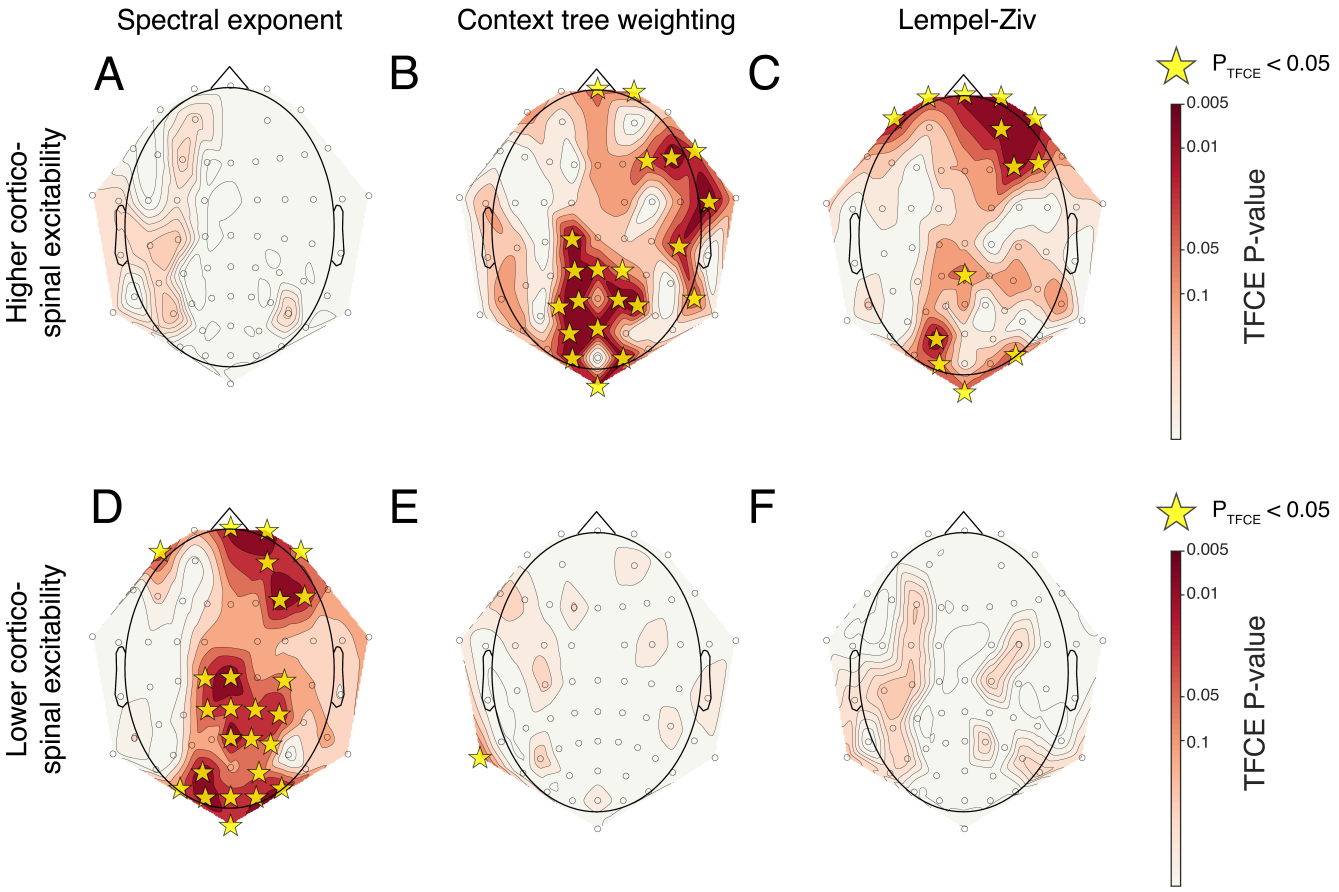

Figure 3. Topographic scalp distributions of TFCE corrected P-values from linear mixed models. EEG entropy was associated with higher CSE (Fig. 3B, C), whereas SE was associated with lower CSE (Fig. 3D). We obtained largely negative findings for increased CSE with SE (Fig. 1A) and decreased CSE with entropy (Fig. 1E,F).

significance or apply TFCE at this stage, as our hypothesis concerned the performance of broadband EEG features above and beyond the benchmark set by band-limited beta EEG features.

Next, we sought to compare broadband EEG features with the performance of beta band-limited EEG features per se, and thus we did not yet add non-EEG fixed effects to LMMs, which might saturate model performance. SE, CTW, and LZ significantly improved the model fit in many channels, including some close to the TMS target region such as C1 and CP1 (Fig. 4D,E,F); SE and LZ also significantly improved the model fit at channel CP3 (Fig. 4D,F). We then added the same non-EEG fixed effects considered previously (Fig. 3) to the base model. While SE and CTW still significantly improved the model fit for channels C1 and CP1 in the vicinity of the TMS target region (Fig. 4G,H), model fits improved by LZ were limited almost exclusively to prefrontal scalp regions and the posterior channel PO3 (Fig. 4I), none of which were in the vicinity of the TMS target region. This result suggests that SE and CTW are preferable over LZ when their performance is considered vis-a-vis the full range of predictive variables. For exact P-values, see Table S2.

Finally, to determine whether broadband EEG measures were primarily trait-markers explaining between-subjects variance or state-markers explaining within-subject variance, we computed the intraclass correlation (ICC) for SE, CTW, LZ, alpha power, and beta power. We did not compute ICCs for alpha or beta phase, because oscillatory phase fluctuates many times per second is thus a state-marker by definition.. The ICC is high when values from within a subject show strong agreement (i.e., low within-subject variance suggestive of a relatively static variable or trait marker) and low when the values from within a subject show weak agreement (i.e., high within-subject variance suggestive of a dynamic variable or state marker). We thus computed a trait-state continuum based on the quantity 1 - ICC (Fig. 5).

Broadband EEG measures SE, CTW, and LZ generally fell closer to the state end of the continuum at most scalp locations (Fig. 5A-C), whereas spectral alpha and beta power generally fell closer to the trait end of the continuum (Fig. 5D,E). The trait-like tendency of spectral power features and state-like ten-

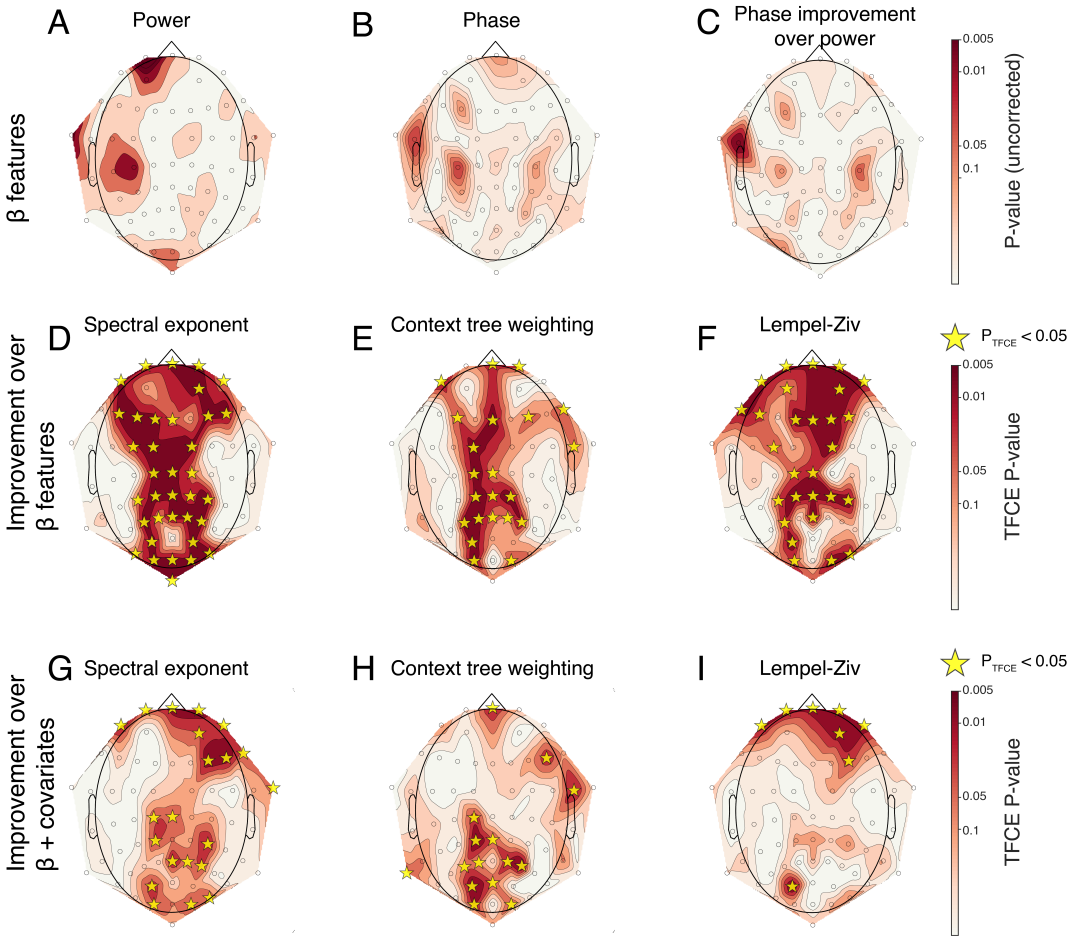

Figure 4. Topographic scalp distributions showing model improvement. Panels A and B show raw P-values from LMMs that predicted MEP amplitude from beta power and phase, respectively. Panel C shows raw P-values from a log-likelihood ratio test of the improvement in model fit from adding beta phase to an LMM with a fixed effect term for beta power. The second row, D - F, shows TFCE-corrected P-values for broadband EEG features used to improve upon the model fit from beta EEG features (log-likelihood ratio tests). The third row shows the results of similar tests where non-EEG fixed effects were added to the base models. Note that we did not consider statistical significance nor apply TFCE to results in the first row as our hypotheses concerned only the performance of broadband EEG features in relation to band-limited beta EEG features.

dency of broadband features were also revealed by histograms (Fig.5F). Overall, CTW appeared to be the most state-like measure. Taken together, the above findings demonstrate that broadband EEG features are relatively dynamic and thus likely to be more sensitive to cortical state changes which can be used to time TMS pulses (e.g., in the context of therapeutic closed loop TMS).

Discussion

In this study, we utilized the 1/f background (spectral exponent, SE) and entropy measures (CTW, LZ) derived from broadband electroencephalogram (EEG) signals to predict corticospinal excitability (CSE). Transcranial magnetic stimulation (TMS) pulses were applied independently of brain state in healthy participants. Our findings indicate that the broadband EEG features (SE, CTW, and LZ) served as effective predictors of CSE, often surpassing the predictive performance of beta EEG phase and power (Fig. 4 D-F), even when additional covariates were accounted for (Fig. 4 G-I). Beta-band EEG power demonstrated the highest topographical specificity as a marker for motor CSE (Fig. 5C). In contrast, SE, CTW, and LZ (Fig. 5D-F) showed more sensitivity to variations in overall brain states compared to either alpha or beta-band EEG power, which appeared more trait-like. The broad-band measures (SE, CTW, and LZ) were more indicative of state changes, as evidenced by lower ICCs, making them suitable for identifying moments of widespread brain excitability. Thus, SE, CTW, and LZ could be invaluable for marking states of brain excitability beyond just the motor cortex. Furthermore, the broadband EEG features we evaluated were measured from roughly 1 s time windows and varied on a slower timescale than EEG phase features which, by definition, fluctuate many times per second. As such, SE, CTW, and LZ might be less susceptible to brief

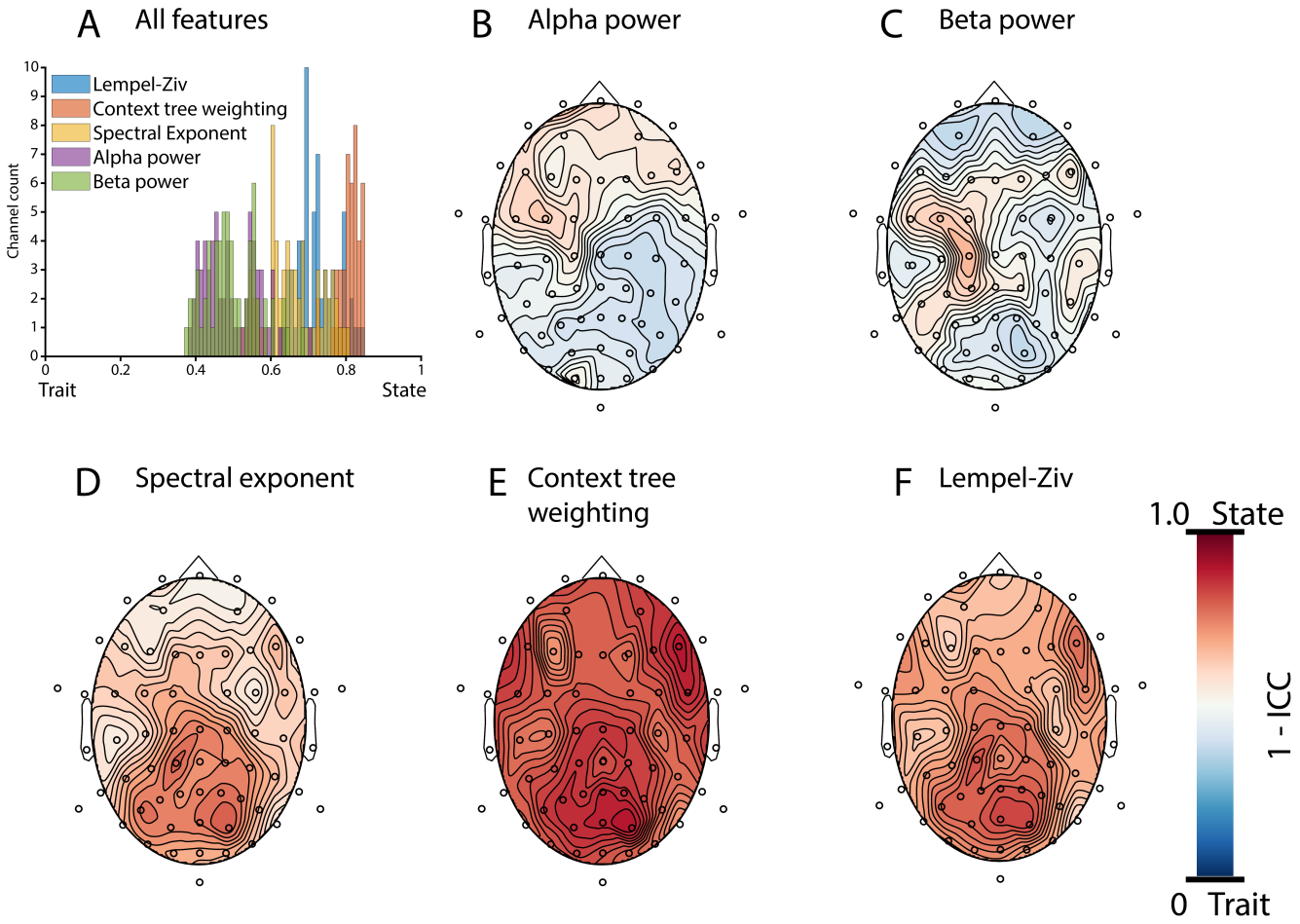

Figure 5. State versus trait features. As judged by the ICC, broadband EEG features appear to be state measures (i.e., more variance within subjects than between subjects at a typical EEG channel, Fig. 5D-F), whereas spectral power EEG features appear to be trait measures, when considering the whole scalp topography (i.e., more variance between subjects than within subjects, Fig. 5B,C). To measure the "stateness" of a feature, we subtracted the intraclass correlation (ICC) from 1, yielding a quantity that is greatest for state measures (red colors in topoplots) and lowest for trait measures (blue colors in topoplots). A histogram of this quantity (Fig. 5A) shows the number of channels for each measure which fall into bins along the trait-state continuum.

physiological artifacts which influence phase estimates.

Broadband EEG measures improve upon CSE prediction from band-limited spectral power. In response to the challenges of band-limited features for CSE prediction , SE, CTW, and LZ offer to eliminate issues stemming from the experimenter's choice of EEG frequency and/or phase (see Introduction). These broadband EEG features may encompass all canonical EEG frequency bands (delta, theta, alpha, beta, and gamma) after high-pass filtering to remove drift artifacts and low-pass filtering to remove EMG artifacts and technical artifacts such as 50 Hz line noise, thus avoiding the pitfalls of a band-limited approach. Two of these broadband EEG features, CTW and LZ, are based on eponymous compression algorithms which quantify the number of unique substrings or states in the signal (24, 48). The other broadband EEG feature, SE, is based on the spectral steepness of the 1/f background of the EEG signal, which has been used a proxy for the ratio of neural excitation to inhibition (37, 39). Because beta EEG features (phase and power) outperformed alpha EEG features in an initial exploratory analysis focused near the TMS target region (Fig. 2), we next used beta EEG features as benchmarks and asked whether adding our alternative, broadband EEG measures could improve the prediction of CSE above and beyond models that already used beta phase and power (Fig. 4 D-F), as well as additional non-EEG covariates (Fig. G-I).

We answered the above question in the affirmative for all three broadband EEG features, albeit in slightly different anatomical scalp regions in each case. When non-EEG covariates were considered, SE and CTW significantly improved the model fit in the vicinity of the left M1 which we targeted with TMS (Fig. 4G,H). This vicinity included channel C1, whose scalp location often coincided with or fell adjacent to the TMS

target region, as well as left centroparietal channels, fitting with another prior study of surface-Laplacian transformed EEG signals (16) which reported that postcentral scalp recordings can be used to predict CSE in a posthoc analysis of data collected during TMS of left M1. As mentioned previously, the relevance of postcentral cortical areas for CSE is also suggested by prior studies showing that the alpha (mu) rhythm, which is hypothesized to gate sensorimotor excitability, has a plausible origin in primary somatosensory cortex (S1), rather than M1 (54–57). Furthermore, the intimate relationship between M1 and S1 is underscored by evidence suggesting that both serve a similar function in early infant development, when M1 primarily receives reafferent signals from twitching limbs before later developing the ability to send motor commands(58–61). This common ontogeny strengthens the plausibility of SE and CTW derived from postcentral areas as useful readouts of CSE.

Different broadband EEG features offer different advantages. LZ showed a more frontal sensitivity when its ability to improve upon benchmark models was considered. Thus, even though LZ considered on its own merits can significantly predict CSE in the vicinity of the TMS target region (Fig. 3C), LZ derived from electrodes in this scalp region does not appear to offer predictive information beyond that obtainable using non-EEG covariates of TMS pulse count, TMS pulse number, and the standard deviation of the EMG signal (Fig. 4I). By contrast, CTW showed a more posterior sensitivity (Fig. 4H), and SE seemed to be predictive of CSE in both frontal and posterior scalp areas (Fig. 4G) when tested against the same benchmark models that included non-EEG covariates. However, future studies which aim to predict CSE from broadband EEG features in realtime applications will likely use a predefined region of interest, in which case the optimal EEG predictor will be the one which gives the strongest prediction when computed from signals recorded in that region. If one selects channels near our TMS target region for this purpose, such as C1 and/or CP1, then CTW and SE appear to perform similarly (Fig. 4, Table S2).

Remarkably, LZ and CTW show quite different sensitives as entropy estimators, despite both being computed from compression algorithms. Why is LZ, unlike CTW, mainly useful as a CSE predictor when computed from prefrontal scalp electrodes? While it is plausible that CSE is influenced by prefrontal disinhibition of motor cortex (e.g., executive control), frontal electrodes may have been contaminated by residual muscle artifacts to a greater extent than centroparietal channels, despite our best efforts to reduce physiological artifacts from EEG signals and to covary for prepulse muscle tone recorded from the right hand. Thus, we are less confident that the LZ finding is truly a neural effect, as opposed to a readout of facial muscle activation. CTW is perhaps a more useful measure of cortical entropy than LZ for the purpose of inferring CSE. This is somewhat surprising, given that both entropy estimates are based on compression algorithms and have performed similarly on neural data in other studies (34, 62–64), and, furthermore, LZ is much more widely applied in human neuroscience across contexts ranging from studies of anesthetics (30, 31, 65, 66), sleep (31, 33, 67, 68) , and pharmacological drug challenge (33, 69, 70), including effects on TMS-evoked potentials (71–73). Nonetheless, from a purely computational perspective, there are strong reasons to believe CTW is a superior entropy estimator for time series data. Unlike LZ, CTW is based on Bayesian inference, which has long been known to produce more data-efficient estimators (74). Accordingly, CTW consistently outperforms other entropy estimators (including LZ) when evaluated on synthetic data (75). This increased data efficiency allowed us to discretize the EEG signal into 8 symbols prior to the calculation of CTW (compared to the LZ calculation with only 2 symbols), such that CTW was able to capture more details of the signal's fine-grained dynamics. Considering the above, we advocate for further use of CTW as an entropy estimator for neural data, not only in TMS-EEG experiments, but also in other EEG analysis contexts.

A new approach for state-dependent TMS. We carried out this study with an eye toward state-dependent TMS applications, e.g., closed-loop TMS, guided by EEG features. As suggested by its name, TMS in this context is automatically triggered by variables which indicate a rapidly fluctuating cortical state. Variables which primarily reflect a trait, rather than dynamic state, are not expected to be useful for state-dependent TMS, given that they are approximately static at the relevant timescale within a given subject.

Given the hierarchical nature of our data, which included many TMS-EEG trials both within and between participants, it was reasonable for us to ask whether our findings were driven primarily by state (within-subject variance) or trait (between-subjects variance). Although the entropy (31–34, 65) and 1/f background (35, 37, 38) of the broadband EEG is already known to change drastically between states of consciousness,

it is currently uncertain to what extent these EEG features change within the awake and alert resting state. To address this uncertainty, we computed ICCs for EEG features and used the quantity $1 - \text{ICC}$ to infer the degree of within-subject variance, with 1 indicating a state variable and 0 indicating a trait variable. We found that broadband EEG features generally showed greater within-subject variance than spectral alpha or beta power. Our results suggest that broadband EEG features are sensitive to cortical states that fluctuate within a TMS-EEG session.

In short, the broadband EEG entropy and 1/f background may be useful for guiding state-dependent TMS. Nonetheless, their usage in state-dependent TMS is not mutually exclusive with that of band-limited EEG measures. Alpha and beta phase, by definition, fluctuate many times per second, and are thus state-markers on a much shorter timescale. As such, they may compliment the usage of broadband EEG measures, which are computed from longer windows of data. Future experiments could trigger realtime TMS by implementing an AND gate with dual criteria: one based on SE or entropy, and another based on phase (e.g., a TMS pulse is fired when both the entropy is high and the phase of beta reaches a trough/rising flank). Indeed, both EEG features might work synergistically together, given that EEG phase is necessarily computed on a very short timescale sensitive to rapid fluctuations, whereas broadband EEG measures would likely be computed on a longer timescale of approximately 1 s and thus be relatively robust to brief signal artifacts. We are also open to realtime TMS triggered using both broadband EEG features and band-limited EEG power features. Such an approach would take advantage of the different information conveyed by each feature type and follow naturally from the prediction of CSE in our current study using models that combined both feature types.

Conclusions, limitations, and future directions . Hitherto, the field of state-dependent TMS has focused almost exclusively on band-limited spectral EEG measures such as alpha and beta power or phase. Our results suggest the utility of new, and perhaps complimentary, broadband EEG measures that improve CSE prediction above and beyond that achieved using band-limited measures. Because these new EEG measures do not require narrowband filtering nor phase estimation/prediction, they are unaffected by many issues which have likely hampered the reproducibility of previous work in this field.

At the same time, we admit that the broadband EEG measures we tested are not parameter free. A symbolic transformation must be applied to EEG signals before LZ or CTW can be used as entropy estimators, and this step could be handled differently by other researchers with respect to the number of symbols and the symbol threshold – although recently proposed methods are able to estimate entropy without requiring discretisation (76). Similarly, other researchers may choose different FOOOF parameters (36) when computing SE, thus introducing further researcher degrees of freedom (77). However, we maintain that these choices are more tractable than the current methodological divergences which impede the field.

Furthermore, although our first pass at data cleaning was handled using an automated procedure with objective criteria (ASR), we also utilized a group-level ICA decomposition for further cleaning (e.g., to remove technical artifacts). Because the ICA decomposition is generally slow and thus cannot be run in realtime, this step may somewhat reduce the translatability of our findings to realtime applications.

Finally, we only tested broadband EEG measures in young, healthy participants. Because therapeutic applications of realtime state-dependent TMS-EEG require EEG features that are useful in clinical populations, a next step will be to repeat our analysis in data from clinical cohorts such as patients recovering from stroke. After we have evaluated these EEG features in clinical subjects, the practical value of these EEG features as dynamic readouts of CSE will ultimately be determined by applications to realtime state-dependent TMS-EEG. Thus, the final step in our line of investigation is to estimate the EEG entropy and 1/f background as TMS triggers in a closed-loop experiment with clinical patients. Given this ultimate goal, we view our current study as a first in a line of research toward developing improved therapeutic TMS-EEG for motor rehabilitation and similar purposes.

Acknowledgements

We sincerely thank all participants who volunteered for our study. We gratefully acknowledge the German Federal Ministry of Education and Research (BMBF) grants Somnia (13GW0294), Enable (13GW0359) and Bevares (13GW0570), and the European Union's Joint Programme for Neurodegenerative Disease Research (EU-JPND 2022-130) grant Recast (01ED2309). We also gratefully acknowledge support from the Open Access Publishing Fund of the University of Tübingen.

Author contributions

JF, SR, and AG conceived the idea for the project. JF wrote the analysis code, analyzed the data, and wrote the first draft of the manuscript. SR guided the analyses and advised the statistical analysis. BT assisted with data collection, as well as MEP data preprocessing and trial rejection. MK advised the analysis and performed the code review. PM advised with the use of entropy measures and provided the code to compute entropy features. AG supervised the project. All authors edited the manuscript.

1. Fatemeh Khademi, Vladislav Royter, Lukas Ziegler, and Alireza Gharabaghi. Resolving equivocal gain modulation of corticospinal excitability. NeuroImage, 269:119891, 2023.
2. Gijs van Elswijk, Femke Maij, Jan-Mathijs Schoffelen, Sebastiaan Overeem, Dick F Stegeman, and Pascal Fries. Corticospinal beta-band synchronization entails rhythmic gain modulation. Journal of Neuroscience, 30(12):4481–4488, 2010.
3. Fatemeh Khademi, Vladimir Royter, and Alireza Gharabaghi. Distinct beta-band oscillatory circuits underlie corticospinal gain modulation. Cerebral Cortex, 28(4):1502–1515, 2018.
4. Georgios Naros, Tobias Lehnertz, Maria Teresa Leão, Ulf Ziemann, and Alireza Gharabaghi. Brain state-dependent gain modulation of corticospinal output in the active motor system. Cerebral Cortex, 30(1):371–381, 2020.
5. Christoph Zrenner, Gábor Kozák, Natalie Schaworonkow, Johanna Metsomaa, David Baur, David Vetter, Daniel M Blumberger, Ulf Ziemann, and Paolo Belardinelli. Corticospinal excitability is highest at the early rising phase of sensorimotor μ-rhythm. NeuroImage, 266: 119805, 2023.
6. Sara J Hussain, Leonardo Claudino, Marlene Bönstrup, Gina Norato, Gabriel Cruciani, Ryan Thompson, Christoph Zrenner, Ulf Ziemann, Ethan Buch, and Leonardo G Cohen. Sensorimotor oscillatory phase–power interaction gates resting human corticospinal output. Cerebral Cortex, 29(9):3766–3777, 2019.
7. Recep A Ozdemir, Sofia Kirkman, Justine R Magnuson, Peter J Fried, Alvaro Pascual-Leone, and Mouhsin M Shafi. Phase matters when there is power: phasic modulation of corticospinal excitability occurs at high amplitude sensorimotor mu-oscillations. Neuroimage: Reports, 2 (4):100132, 2022.
8. Andrea Guerra, Alek Pogosyan, Magdalena Nowak, Huiling Tan, Florinda Ferreri, Vincenzo Di Lazzaro, and Peter Brown. Phase dependency of the human primary motor cortex and cholinergic inhibition cancelation during beta tacs. Cerebral Cortex, 26(10):3977–3990, 2016.
9. Valerio Raco, Robert Bauer, Srikandarajah Tharsan, and Alireza Gharabaghi. Combining tms and tacs for closed-loop phase-dependent modulation of corticospinal excitability: a feasibility study. Frontiers in cellular neuroscience, 10:143, 2016.
10. Lukas Schilberg, Tahnée Engelen, Sanne Ten Oever, Teresa Schuhmann, Beatrice De Gelder, Tom A de Graaf, and Alexander T Sack. Phase of beta-frequency tacs over primary motor cortex modulates corticospinal excitability. cortex, 103:142–152, 2018.
11. Hisato Nakazono, Katsuya Ogata, Tsuyoshi Kuroda, and Shozo Tobimatsu. Phase and frequency-dependent effects of transcranial alternating current stimulation on motor cortical excitability. PLoS One, 11(9):e0162521, 2016.
12. Miles Wischnewski, Harry Tran, Zhihe Zhao, Sina Shirinpour, Zachary J Haigh, Jonna Rotteveel, Ivan Alekseichuk, Jan Zimmermann, and Alexander Opitz. Induced neural phase precession through exogeneous electric fields. bioRxiv, pages 2023–03, 2023.
13. Christoph Zrenner, Debora Desideri, Paolo Belardinelli, and Ulf Ziemann. Real-time eeg-defined excitability states determine efficacy of tms-induced plasticity in human motor cortex. Brain stimulation, 11(2):374–389, 2018.
14. Kristoffer Hougaard Madsen, Anke Ninija Karabanov, Lærke Gebser Krohne, Mads Gylling Safeldt, Leo Tomasevic, and Hartwig Roman Siebner. No trace of phase: Corticomotor excitability is not tuned by phase of pericentral mu-rhythm. Brain stimulation, 12(5):1261–1270, 2019.
15. Fatemeh Khademi, Vladislav Royter, and Alireza Gharabaghi. State-dependent brain stimulation: power or phase? Brain stimulation, 12(2):296–299, 2019.
16. Anke Ninija Karabanov, Kristoffer Hougaard Madsen, Lærke Gebser Krohne, and Hartwig Roman Siebner. Does pericentral mu-rhythm "power" corticomotor excitability?–a matter of eeg perspective. Brain stimulation, 14(3):713–722, 2021.
17. Tharan Suresh and Sara J Hussain. Re-evaluating the contribution of sensorimotor mu rhythm phase and power to human corticospinal output: A replication study. Brain Stimulation: Basic, Translational, and Clinical Research in Neuromodulation, 2023.
18. Til Ole Bergmann, Anne Lieb, Christoph Zrenner, and Ulf Ziemann. Pulsed facilitation of corticospinal excitability by the sensorimotor μ-alpha rhythm. Journal of Neuroscience, 39 (50):10034–10043, 2019.
19. Miles Wischnewski, Zachary J Haigh, Sina Shirinpour, Ivan Alekseichuk, and Alexander Opitz. The phase of sensorimotor mu and beta oscillations has the opposite effect on corticospinal excitability. Brain Stimulation, 15(5):1093–1100, 2022.
20. Christoph Zrenner, Paolo Belardinelli, Maria Ermolova, Pedro Caldana Gordon, Matti Stenroos, Brigitte Zrenner, and Ulf Ziemann. μ-rhythm phase from somatosensory but not motor cortex correlates with corticospinal excitability in eeg-triggered tms. Journal of Neuroscience Methods, 379:109662, 2022.
21. Robert Guggenberger, Julian-Samuel Gebuehr, Marius Keute, and Alireza Gharabaghi. Phase-specific stimulation of the human brain with real-time measurement instead of prediction. bioRxiv, pages 2023–04, 2023.
22. Marius Keute, Julian-Samuel Gebuehr, Robert Guggenberger, Bettina Hanna Trunk, and Alireza Gharabaghi. Phase-specific stimulation reveals consistent sinusoidal modulation of human corticospinal excitability along the oscillatory beta cycle. bioRxiv, pages 2023–04, 2023.
23. Flavie Torrecillos, Emma Falato, Alek Pogosyan, Timothy West, Vincenzo Di Lazzaro, and Peter Brown. Motor cortex inputs at the optimum phase of beta cortical oscillations undergo more rapid and less variable corticospinal propagation. Journal of Neuroscience, 40(2): 369–381, 2020.
24. Abraham Lempel and Jacob Ziv. On the complexity of finite sequences. IEEE Transactions on information theory, 22(1):75–81, 1976.
25. Frans MJ Willems, Yuri M Shtarkov, and Tjalling J Tjalkens. The context-tree weighting method: Basic properties. IEEE transactions on information theory, 41(3):653–664, 1995.
26. Giulio Tononi and Gerald M Edelman. Consciousness and complexity. science, 282(5395): 1846–1851, 1998.
27. Giulio Tononi, Melanie Boly, Marcello Massimini, and Christof Koch. Integrated information theory: from consciousness to its physical substrate. Nature Reviews Neuroscience, 17(7): 450–461, 2016.
28. Robin Lester Carhart-Harris, Robert Leech, Peter John Hellyer, Murray Shanahan, Amanda Feilding, Enzo Tagliazucchi, Dante R Chialvo, and David Nutt. The entropic brain: a theory of conscious states informed by neuroimaging research with psychedelic drugs. Frontiers in human neuroscience, page 20, 2014.
29. Robin L Carhart-Harris. The entropic brain-revisited. Neuropharmacology, 142:167–178, 2018.
30. X-S Zhang, Rob J Roy, and Erik W Jensen. Eeg complexity as a measure of depth of anesthesia for patients. IEEE transactions on biomedical engineering, 48(12):1424–1433, 2001.
31. Adenauer G Casali, Olivia Gosseries, Mario Rosanova, Mélanie Boly, Simone Sarasso, Karina R Casali, Silvia Casarotto, Marie-Aurélie Bruno, Steven Laureys, Giulio Tononi, et al. A theoretically based index of consciousness independent of sensory processing and behavior. Science translational medicine, 5(198):198ra105–198ra105, 2013.
32. Anthony G Hudetz, Xiping Liu, Siveshigan Pillay, Melanie Boly, and Giulio Tononi. Propofol anesthesia reduces lempel-ziv complexity of spontaneous brain activity in rats. Neuroscience letters, 628:132–135, 2016.
33. Michael M Schartner, Robin L Carhart-Harris, Adam B Barrett, Anil K Seth, and Suresh D Muthukumaraswamy. Increased spontaneous meg signal diversity for psychoactive doses of ketamine, lsd and psilocybin. Scientific reports, 7(1):46421, 2017.
34. Joel Frohlich, Jeffrey N Chiang, Pedro AM Mediano, Mark Nespeca, Vidya Saravanapandian, Daniel Toker, John Dell'Italia, Joerg F Hipp, Shafali S Jeste, Catherine J Chu, et al. Neural complexity is a common denominator of human consciousness across diverse regimes of cortical dynamics. Communications Biology, 5(1):1374, 2022.
35. Michele Angelo Colombo, Martino Napolitani, Melanie Boly, Olivia Gosseries, Silvia Casarotto, Mario Rosanova, Jean-Francois Brichant, Pierre Boveroux, Steffen Rex, Steven Laureys, et al. The spectral exponent of the resting eeg indexes the presence of consciousness during unresponsiveness induced by propofol, xenon, and ketamine. NeuroImage, 189:631–644, 2019.
36. Thomas Donoghue, Matar Haller, Erik J Peterson, Paroma Varma, Priyadarshini Sebastian, Richard Gao, Torben Noto, Antonio H Lara, Joni D Wallis, Robert T Knight, et al. Parameterizing neural power spectra into periodic and aperiodic components. Nature neuroscience, 23 (12):1655–1665, 2020.
37. Richard Gao, Erik J Peterson, and Bradley Voytek. Inferring synaptic excitation/inhibition balance from field potentials. Neuroimage, 158:70–78, 2017.
38. Janna D Lendner, Randolph F Helfrich, Bryce A Mander, Luis Romundstad, Jack J Lin, Matthew P Walker, Pal G Larsson, and Robert T Knight. An electrophysiological marker of arousal level in humans. Elife, 9:e55092, 2020.
39. Christoph Wiest, Flavie Torrecillos, Alek Pogosyan, Manuel Bange, Muthuraman Muthuraman,

Sergiu Groppa, Natasha Hulse, Harutomo Hasegawa, Keyoumars Ashkan, Fahd Baig, et al. The aperiodic exponent of subthalamic field potentials reflects excitation/inhibition balance in parkinsonism. Elife, 12:e82467, 2023.

40. Simone Rossi, Andrea Antal, Sven Bestmann, Marom Bikson, Carmen Brewer, Jürgen Brockmöller, Linda L Carpenter, Massimo Cincotta, Robert Chen, Jeff D Daskalakis, et al. Safety and recommendations for tms use in healthy subjects and patient populations, with updates on training, ethical and regulatory issues: Expert guidelines. Clinical Neurophysiology, 132(1):269–306, 2021.
41. S Groppa, A Oliviero, A Eisen, Angelo Quartarone, LG Cohen, V Mall, A Kaelin-Lang, T Mima, Serena Rossi, GW Thickbroom, et al. A practical guide to diagnostic transcranial magnetic stimulation: report of an ifcn committee. Clinical Neurophysiology, 123(5):858–882, 2012.
42. Tim Mullen, Christian Kothe, Yu Mike Chi, Alejandro Ojeda, Trevor Kerth, Scott Makeig, Gert Cauwenberghs, and Tzyy-Ping Jung. Real-time modeling and 3d visualization of source dynamics and connectivity using wearable eeg. In 2013 35th annual international conference of the IEEE engineering in medicine and biology society (EMBC), pages 2184–2187. IEEE, 2013.
43. Arnaud Delorme and Scott Makeig. Eeglab: an open source toolbox for analysis of single-trial eeg dynamics including independent component analysis. Journal of neuroscience methods, 134(1):9–21, 2004.
44. Gyorgy Buzsaki. Rhythms of the Brain. Oxford university press, 2006.
45. György Buzsáki and Kenji Mizuseki. The log-dynamic brain: how skewed distributions affect network operations. Nature Reviews Neuroscience, 15(4):264–278, 2014.
46. Claude E Shannon. A mathematical theory of communication. The Bell system technical journal, 27(3):379–423, 1948.
47. Thomas M Cover. Elements of information theory. John Wiley & Sons, 1999.
48. Ron Begleiter, Ran El-Yaniv, and Golan Yona. On prediction using variable order markov models. Journal of Artificial Intelligence Research, 22:385–421, 2004.
49. Stephen M Smith and Thomas E Nichols. Threshold-free cluster enhancement: addressing problems of smoothing, threshold dependence and localisation in cluster inference. Neuroimage, 44(1):83–98, 2009.
50. Armand Mensen and Ramin Khatami. Advanced eeg analysis using threshold-free cluster-enhancement and non-parametric statistics. Neuroimage, 67:111–118, 2013.
51. Eric Maris and Robert Oostenveld. Nonparametric statistical testing of eeg-and meg-data. Journal of neuroscience methods, 164(1):177–190, 2007.
52. Kenneth O McGraw and Seok P Wong. Forming inferences about some intraclass correlation coefficients. Psychological methods, 1(1):30, 1996.
53. Arash Salarian. Intraclass Correlation Coefficient (ICC), November 2016. URL https://www.mathworks.com/matlabcentral/fileexchange/22099-intraclass-correlation-coefficient-icc. Version 1.3.1.0 (2.45 KB).
54. Riitta Salmelin and Riitta Hari. Spatiotemporal characteristics of sensorimotor neuromagnetic rhythms related to thumb movement. Neuroscience, 60(2):537–550, 1994.
55. Jaime A Pineda. The functional significance of mu rhythms: translating “seeing” and “hearing” into “doing”. Brain research reviews, 50(1):57–68, 2005.
56. JJ Bouyer, C Tilquin, and A Rougeul. Thalamic rhythms in cat during quiet wakefulness and immobility. Electroencephalography and clinical neurophysiology, 55(2):180–187, 1983.
57. Petra Ritter, Matthias Moosmann, and Arno Villringer. Rolandic alpha and beta eeg rhythms’ strengths are inversely related to fmri-bold signal in primary somatosensory and motor cortex. Human brain mapping, 30(4):1168–1187, 2009.
58. Mark S Blumberg, James C Dooley, and Greta Sokoloff. The developing brain revealed during sleep. Current opinion in physiology, 15:14–22, 2020.
59. Alexandre Tiriac, Carlos Del Rio-Bermudez, and Mark S Blumberg. Self-generated movements with “unexpected” sensory consequences. Current Biology, 24(18):2136–2141, 2014.
60. James C Dooley and Mark S Blumberg. Developmental’awakening’of primary motor cortex to the sensory consequences of movement. elife, 7:e41841, 2018.
61. Mark S Blumberg and Karen E Adolph. Protracted development of motor cortex constrains rich interpretations of infant cognition. Trends in Cognitive Sciences, 2023.
62. Pedro AM Mediano, Aleksi Ikkala, Rogier A Kievit, Sridhar R Jagannathan, Thomas F Varley, Emmanuel A Stamatakis, Tristan A Bekinschtein, and Daniel Bor. Fluctuations in neural complexity during wakefulness relate to conscious level and cognition. BioRxiv, pages 2021–09, 2021.
63. Fernando E Rosas, Pedro AM Mediano, Christopher Timmermann, Andrea I Luppi, Diego Candia-Rivera, Reza Abbasi-Asl, Adam Gazzaley, Morten L Kringelbach, Suresh Daniel Muthukumaraswamy, Daniel Bor, et al. The entropic heart: Tracking the psychedelic state via heart rate dynamics. bioRxiv, pages 2023–11, 2023.
64. Joel Frohlich, Julia Moser, Katrin Sippel, Pedro AM Mediano, Hubert Preissl, and Alireza Gharabaghi. Sex differences in prenatal development of neural complexity in the human brain. Nature Mental Health, 2024, https://doi.org/10.1038/s44220-024-00206-4. Accepted for publication on 22 Jan 2024.
65. Simone Sarasso, Melanie Boly, Martino Napolitani, Olivia Gosseries, Vanessa Charland-Verville, Silvia Casarotto, Mario Rosanova, Adenauer Girardi Casali, Jean-Francois Brichant, Pierre Boveroux, et al. Consciousness and complexity during unresponsiveness induced by propofol, xenon, and ketamine. Current Biology, 25(23):3099–3105, 2015.
66. Michael Schartner, Anil Seth, Quentin Noirhomme, Melanie Boly, Marie-Aurelie Bruno, Steven Laureys, and Adam Barrett. Complexity of multi-dimensional spontaneous eeg decreases during propofol induced general anaesthesia. PloS one, 10(8):e0133532, 2015.
67. Arnfinn Aamodt, André Sevenius Nilsen, Rune Markhus, Anikó Kusztor, Fatemeh Hasan-zadehMoghadam, Nils Kauppi, Benjamin Thürer, Johan Frederik Storm, and Bjørn Erik Juel. Eeg lempel-ziv complexity varies with sleep stage, but does not seem to track dream experience. Frontiers in Human Neuroscience, 16, 2022.
68. Benjamin Baird, Giulio Tononi, and Stephen LaBerge. Lucid dreaming occurs in activated rapid eye movement sleep, not a mixture of sleep and wakefulness. Sleep, 45(4):zsab294, 2022.
69. Christopher Timmermann, Leor Roseman, Sharad Haridas, Fernando E Rosas, Lisa Luan, Hannes Kettner, Jonny Martell, David Erritzoe, Enzo Tagliazucchi, Carla Pallavicini, et al. Human brain effects of dmt assessed via eeg-fmri. Proceedings of the National Academy of Sciences, 120(13):e2218949120, 2023.
70. Conor H. Murray, Joel Frohlich, Connor J. Haggarty, Ilaria Tare, Royce Lee, and Harriet de Wit. Neural complexity is increased after low doses of lsd, but not moderate to high doses of oral thc or methamphetamine. Neuropsychopharmacology, 2024. ISSN 1740-634X. . URL https://doi.org/10.1038/s41386-024-01809-2.
71. Nadine Farnes, Bjørn E Juel, André S Nilsen, Luis G Romundstad, and Johan F Storm. Increased signal diversity/complexity of spontaneous eeg, but not evoked eeg responses, in ketamine-induced psychedelic state in humans. Plos one, 15(11):e0242056, 2020.
72. G Darmani, JO Nieminen, TO Bergmann, H Ramezanpour, and U Ziemann. A degraded state of consciousness in healthy awake humans? Brain Stimulation: Basic, Translational, and Clinical Research in Neuromodulation, 14(3):710–712, 2021.
73. Andres Ort, John W Smallridge, Simone Sarasso, Silvia Casarotto, Robin von Rotz, Andrea Casanova, Erich Seifritz, Katrin H Preller, Giulio Tononi, and Franz X Vollenweider. Tms-eeg and resting-state eeg applied to altered states of consciousness: oscillations, complexity, and phenomenology. Iscience, 26(5), 2023.
74. Ilya Nemenman, Fariel Shafee, and William Bialek. Entropy and inference, revisited. Advances in Neural Information Processing Systems, 14, 2001.
75. Yun Gao, Ioannis Kontoyiannis, and Elie Bienenstock. Estimating the entropy of binary time series: Methodology, some theory and a simulation study. Entropy, 10(2):71–99, 2008.
76. Pedro AM Mediano, Fernando E Rosas, Andrea I Luppi, Valdas Noreika, Anil K Seth, Robin L Carhart-Harris, Lionel Barnett, and Daniel Bor. Spectrally and temporally resolved estimation of neural signal diversity. eLife.
77. Joseph P Simmons, Leif D Nelson, and Uri Simonsohn. False-positive psychology: Undisclosed flexibility in data collection and analysis allows presenting anything as significant. Psychological Science, 22(11):1359–1366, 2011.

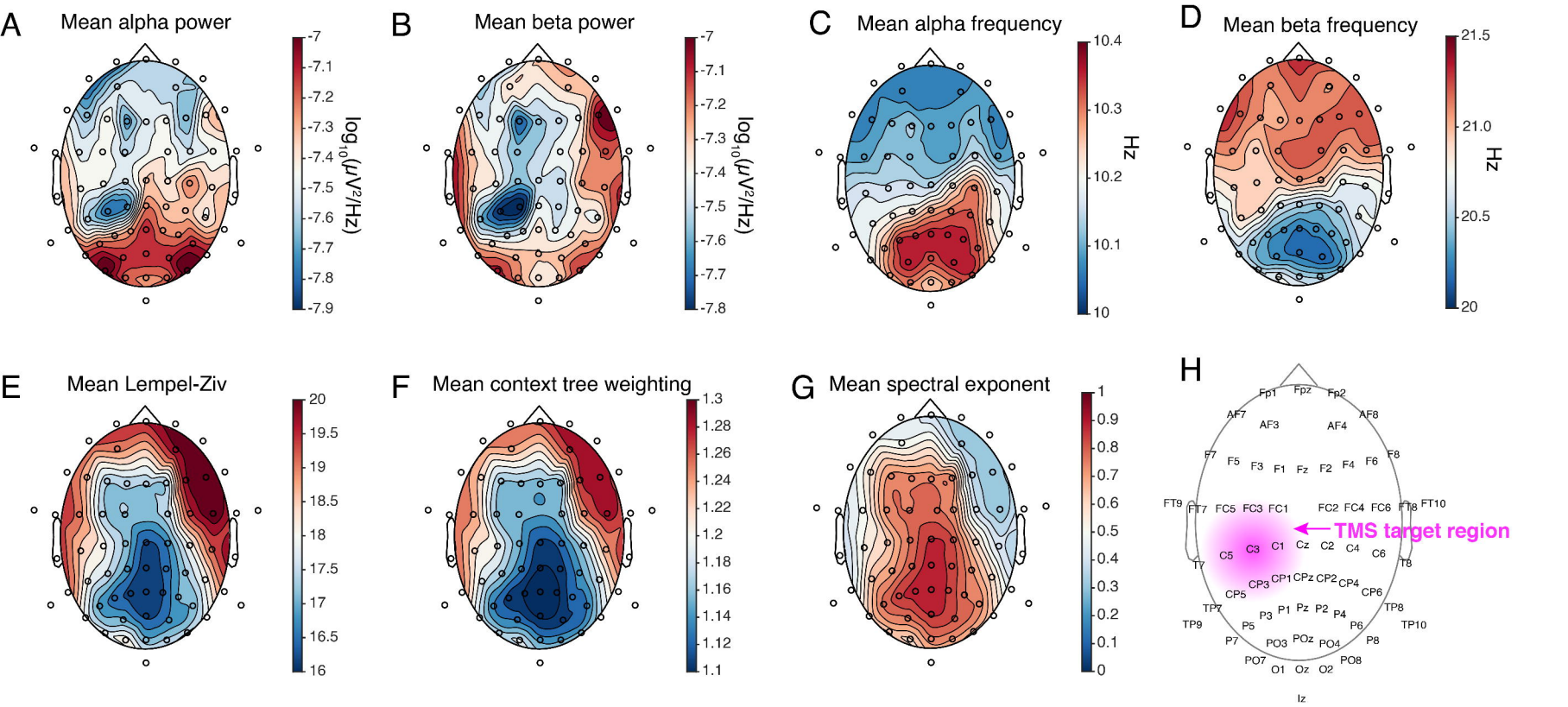
A
Mean alpha power
-7
-7.1
-7.2
-7.3
-7.4
-7.5
-7.6
-7.7
-7.8
-7.9
log10(μV²/Hz)
B
Mean beta power
-7
-7.1
-7.2
-7.3
-7.4
-7.5
-7.6
-7.7
-7.8
log10(μV²/Hz)
C
Mean alpha frequency
10.4
10.3
10.2
10.1
10
Hz
D
Mean beta frequency
21.5
21.0
20.5
20
Hz
E
Mean Lempel-Ziv
20
19.5
19
18.5
18
17.5
17
16.5
16
F
Mean context tree weighting
1.3
1.28
1.26
1.24
1.22
1.2
1.18
1.16
1.14
1.12
1.1
G
Mean spectral exponent
1
0.9
0.8
0.7
0.6
0.5
0.4
0.3
0.2
0.1
0
H
Fp1
Fpz
Fp2
AF7
AF3
AF4
AF8
F7
F5
F3
F1
Fz
F2
F4
F6
F8
FT9
FT7
FC5
FC3
FC1
FC2
FC4
FC6
FT8
FT10
TMS target region
T7
C5
C3
C1
Cz
C2
C4
C6
T8
CP5
CP3
CP1
CPz
CP2
CP4
CP6
TP7
P3
P1
Pz
P2
P4
TP8
TP9
P5
P6
TP10
P7
PO3
POz
PO4
P8
PO7
O1
Oz
O2
PO8
Iz

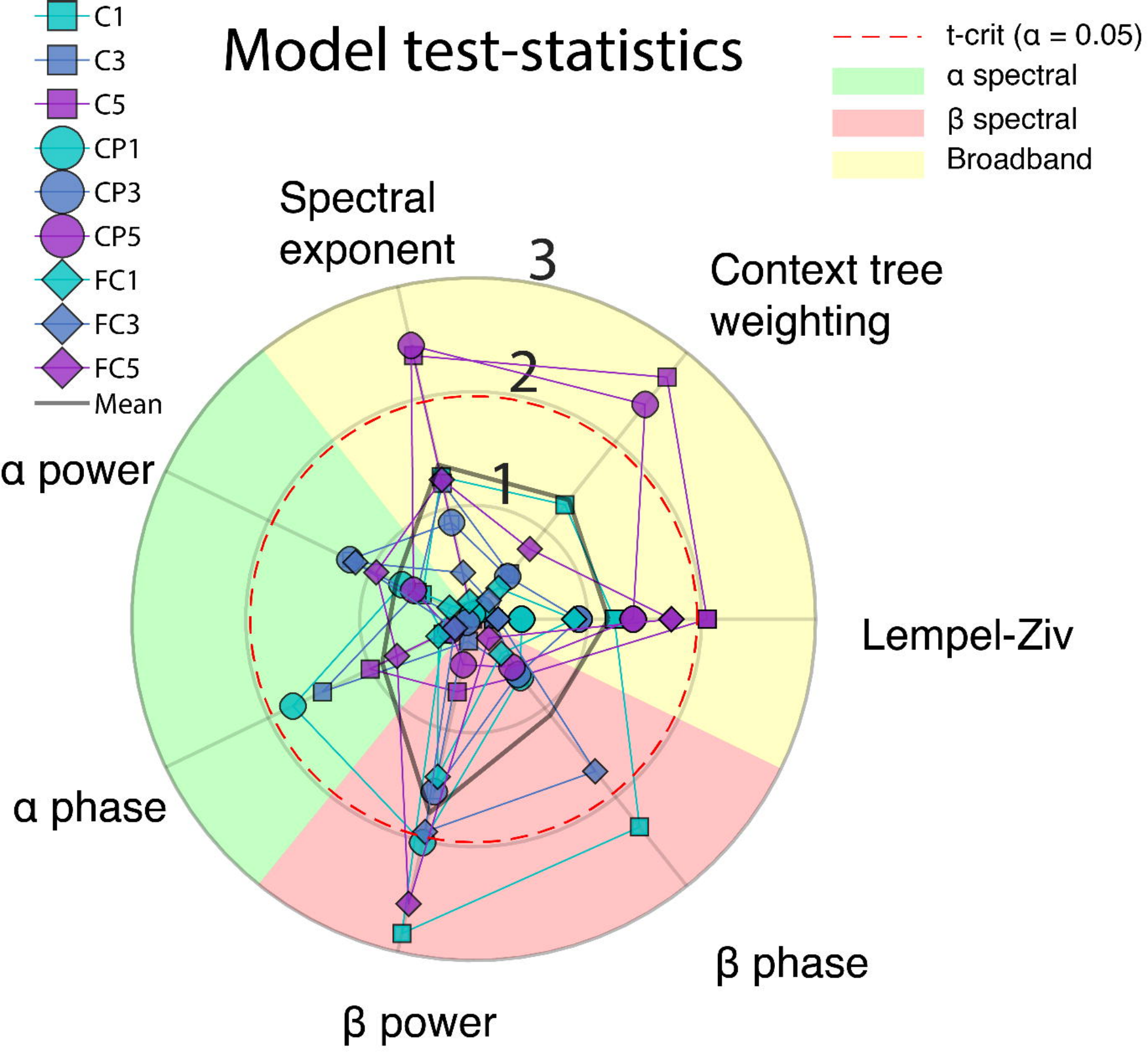
Model test-statistics
t-crit (α = 0.05)
α spectral
β spectral
Broadband
C1
C3
C5
CP1
CP3
CP5
FC1
FC3
FC5
Mean
Spectral exponent
3
2
1
Context tree weighting
Lempel-Ziv
β phase
β power
α phase
α power

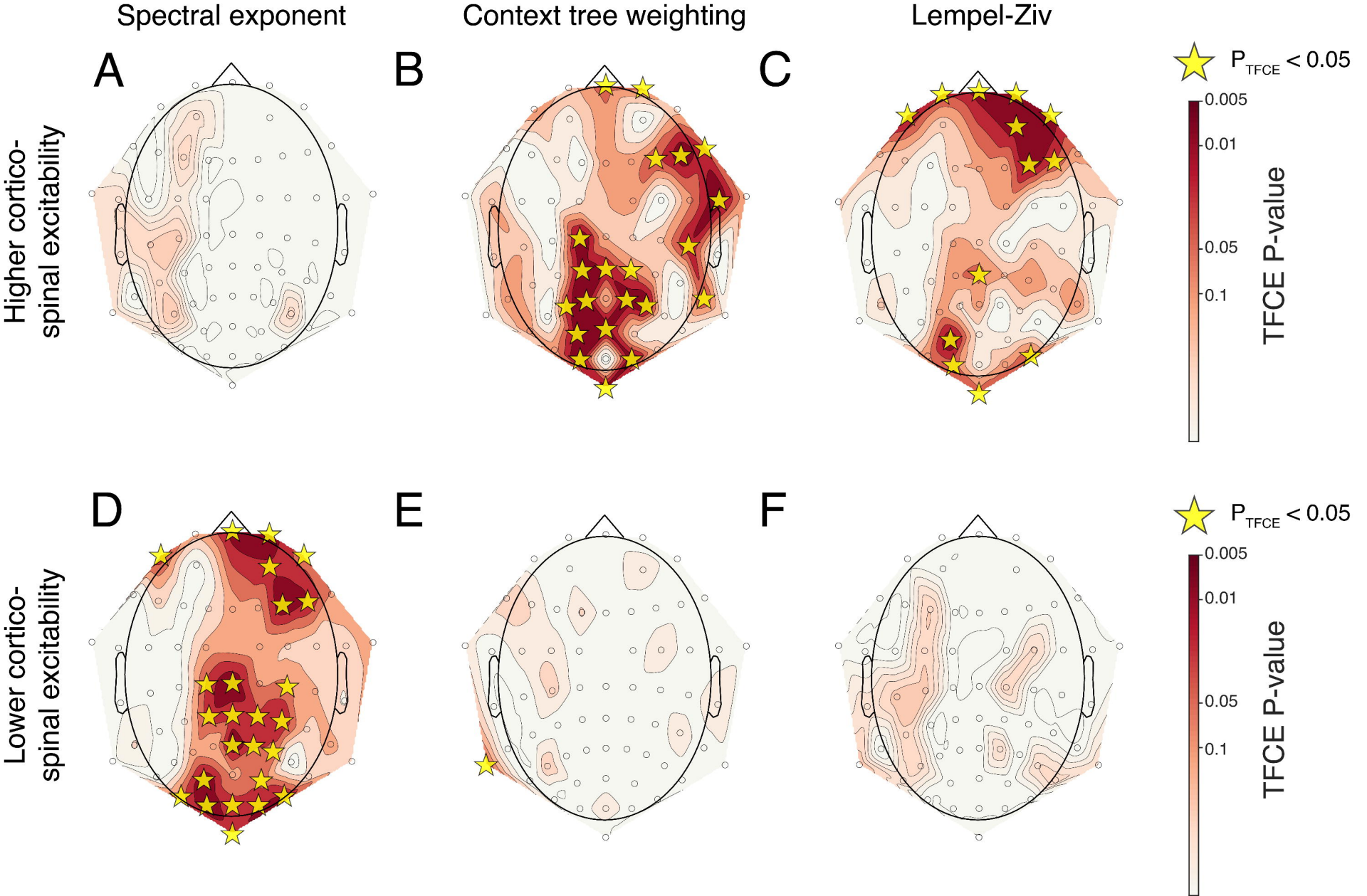
Spectral exponent
Context tree weighting
Lempel-Ziv
A
B
C
D
E
F
Higher cortico-spinal excitability
Lower cortico-spinal excitability
P TFCE < 0.05
0.005
0.01
0.05
0.1
TFCE P-value
P TFCE < 0.05
0.005
0.01
0.05
0.1
TFCE P-value

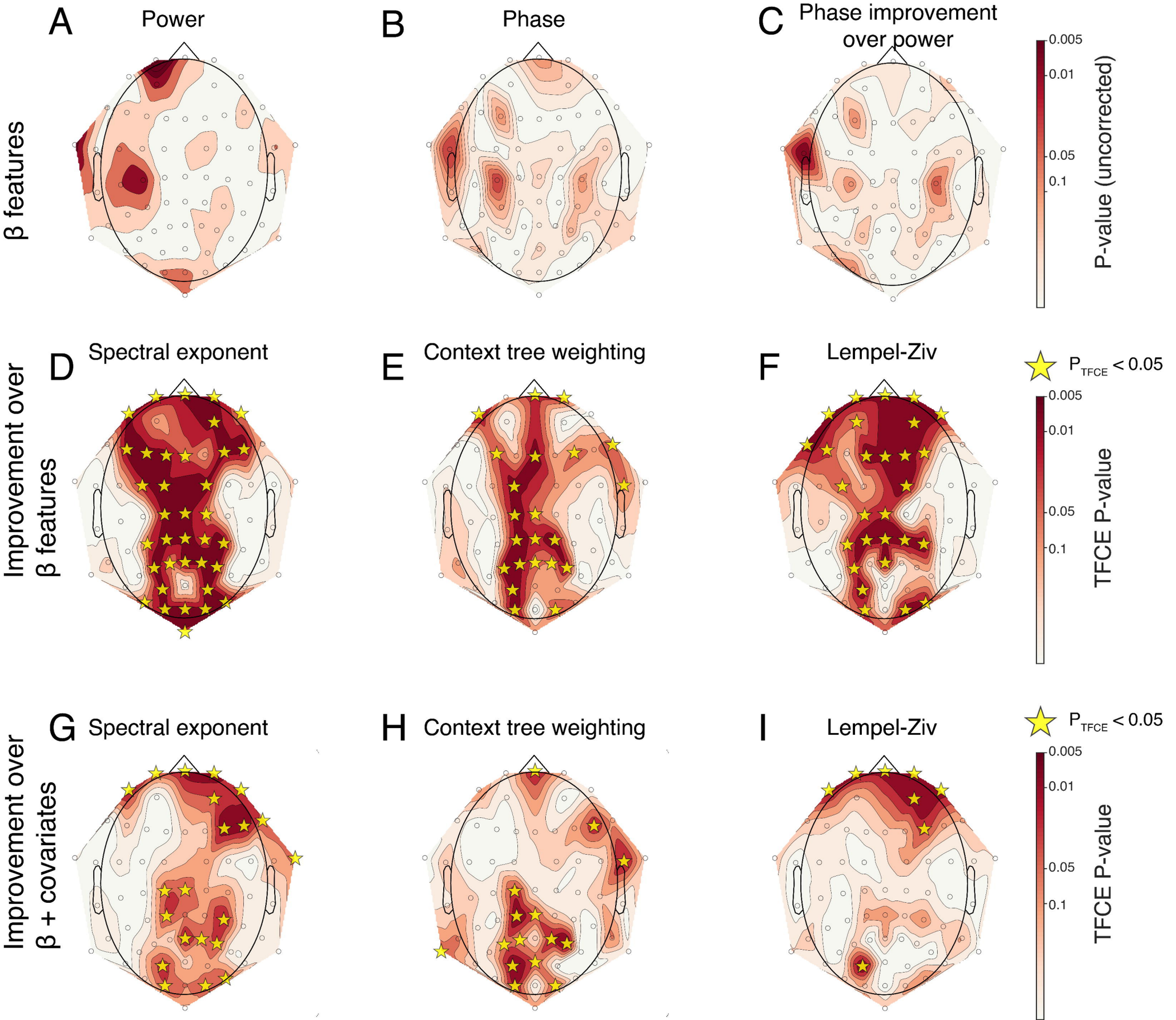
A
Power
B
Phase
C
Phase improvement over power
β features
0.005
0.01
0.05
0.1
P-value (uncorrected)
D
Spectral exponent
E
Context tree weighting
F
Lempel-Ziv
Improvement over β features
$P_{TFCE} < 0.05$
0.005
0.01
0.05
0.1
TFCE P-value
G
Spectral exponent
H
Context tree weighting
I
Lempel-Ziv
Improvement over β + covariates
$P_{TFCE} < 0.05$
0.005
0.01
0.05
0.1
TFCE P-value

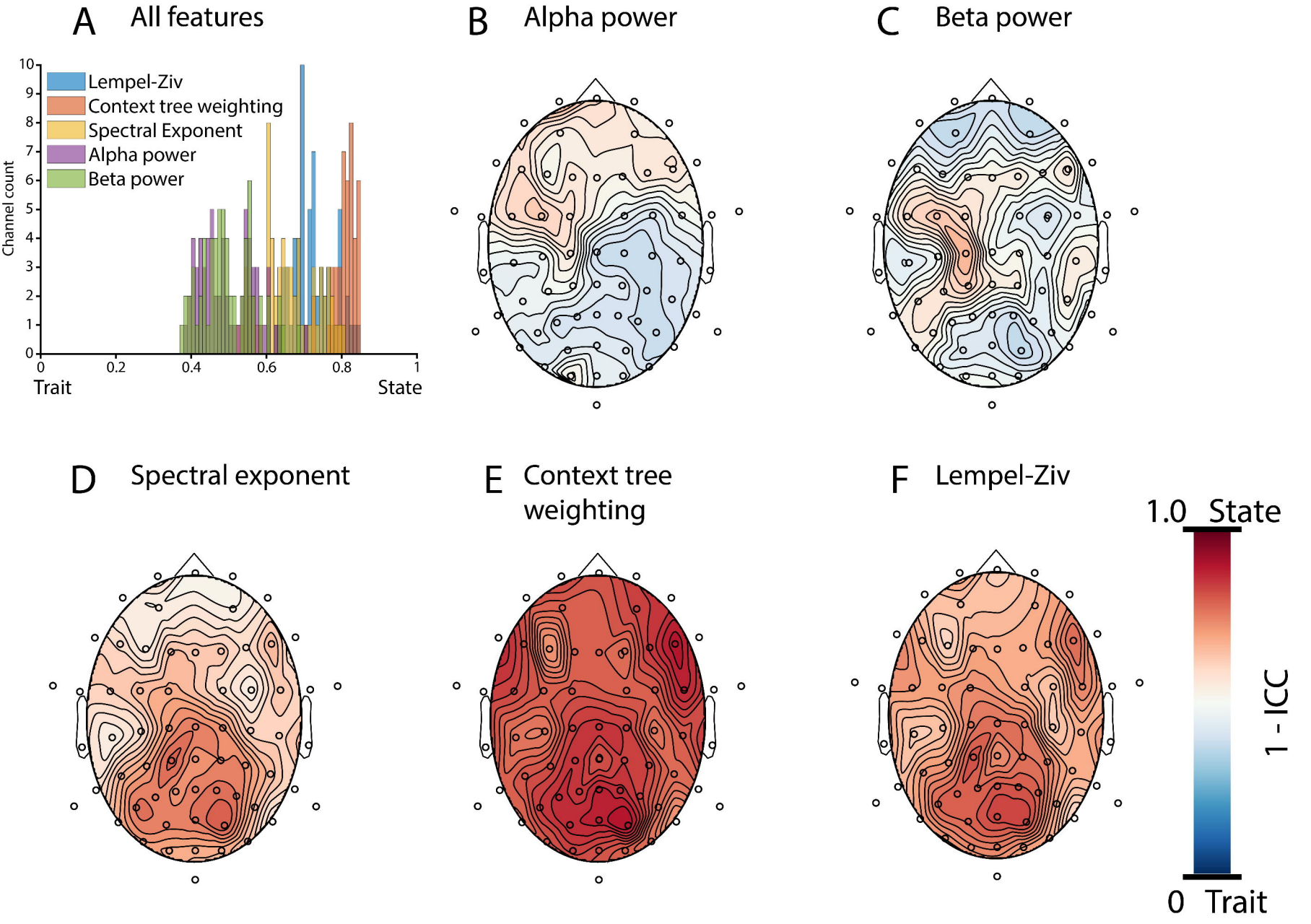
A
All features
Lempel-Ziv
Context tree weighting
Spectral Exponent
Alpha power
Beta power
Channel count
0
1
2
3
4
5
6
7
8
9
10
0
0.2
0.4
0.6
0.8
1
Trait
State
B
Alpha power
C
Beta power
D
Spectral exponent
E
Context tree weighting
F
Lempel-Ziv
1.0 State
1 - ICC
0 Trait